Molecular Dynamics of the Anti-Fluorescein 4−4−20 Antigen-Binding Fragment. 1. Computer Simulations†

Kap Lim‡ and James N. Herron*

Departments of Pharmaceutics and Bioengineering, University of Utah, Salt Lake City, Utah 84112

Received September 21, 1994; Revised Manuscript Received February 28, 1995®

ABSTRACT: Two 174 ps molecular dynamics simulations of the solvated, 4−4−20 antigen-binding fragment (Fab) were performed: one with antigen (fluorescein) in the antigen-combining site and another with it removed. At the beginning of the second simulation, fluorescein was relocated from the antigen-combining site to a point outside the cutoff distance for nonbonded interactions by applying a "pulling force". Initially, the antigen-combining site collapsed when fluorescein was removed but gradually re-formed as the simulation progressed. In addition, several other differences were observed between the two simulations. These included (i) structural rearrangements of key contact residues in the antigen-combining site, (ii) significant differences in the degree of hydration of the antigen-combining site, (iii) a more acute elbow bend angle in the case of the unliganded form, and (iv) less correlated motions of amino acid residues in the unliganded form. These observations suggested that the Fab without fluorescein exhibited a greater degree of segmental flexibility than the Fab with fluorescein. Time-resolved fluorescence experiments were performed in order to validate this prediction, and the results are described in the following paper [Lim *et al.* (1995) *Biochemistry 34,* 6975−6984].

Immunologists have long been interested in whether the antigen−antibody complex forms between two static partners ("lock and key" hypothesis) or whether the antigen and antibody can change their conformations to achieve greater complementarity ("induced-fit" hypothesis) (Berzofsky, 1985). One way to address this issue is to compare the three-dimensional structures of the native and bound forms of the same antigen−antibody complex. Six such structures have been reported in the past few years (Alzari *et al.*, 1990; Stanfield *et al.*, 1990; Herron *et al.*, 1991; Rini *et al.*, 1992; Arevalo *et al.*, 1993; Jeffrey *et al.*, 1993). The first of these studies was published in 1990 by Wilson's group at Scripps. In this study, an antigen-binding fragment (Fab)[1] which bound a synthetic oligopeptide derived from myohemerythrin was crystallized with and without the peptide (Stanfield *et al.*, 1990). No significant conformational changes were observed between the two structures, as was also the case in a study from Poljak's group at the Pasteur Institute, which described the native and bound forms of a Fab fragment which binds 2-phenyloxazone, a small haptenic antigen (Alzari *et al.*, 1990). More recently, similar results were obtained by Jeffrey *et al.* (1993) for the Fab fragment of another anti-hapten antibody (26−10) that binds digoxin. The first study to report an induced-fit mechanism in an antigen-binding fragment was our own paper describing the native and bound forms of the BV04-01 Fab in complex with a trimer of thymidylic acid (Herron *et al.*, 1991). Since then, Wilson's group reported another Fab−peptide complex in which an induced-fit mechanism was observed (Rini *et al.*, 1992). In this case, synthetic peptides from influenza hemagglutinin were used to elicit the antibody. Most recently, Wilson's group reported structures for the unliganded and liganded forms of the DB3 Fab fragment which binds progesterone. They observed that a tryptophan residue in the third complementarity-determining region of the heavy chain (H_3) occupied the binding site in the absence of hapten but moved out of the way in the liganded form (Arevalo *et al.*, 1993)—very similar to the motion of a tryptophan residue in H_3 of BV04-01. Thus, it appears that both lock and key and induced-fit mechanisms have their place in antigenic recognition. However, it is still unclear whether all antibodies are capable of performing the conformational changes required for induced fit or if such changes are limited to a subset of immunoglobulin variable region genes.

In addition to BV04-01, our laboratory has also investigated the induced-fit mechanism in a high-affinity antibody (4−4−20) which binds the fluorescent hapten fluorescein. Monoclonal anti-fluorescein antibodies have been used for the last decade as a model system for studying molecular recognition in the immune system. A wide variety of topics have been investigated including (i) antigen-binding affinity under different conditions (Kranz *et al.*, 1982; Herron, 1984; Gibson *et al.*, 1988; Omelyanenko *et al.*, 1993), (ii) antigen-

† This work was supported in part by USPHS Grant AI 22898, the Center for Biopolymers at Interfaces at the University of Utah, and the Utah Supercomputing Institute. We thank Silicon Graphics, Inc., and BIOSYM Technologies, Inc., for their generous contributions.

‡ Present address: ES 76 Biophysics Branch, George C. Marshall Space Flight Center, NASA, Huntsville, AL 35812.

® Abstract published in *Advance ACS Abstracts,* May 1, 1995.

[1] Abbreviations: 4−4−20, high-affinity murine monoclonal anti-fluorescein antibody; Arg, arginine; C_α, α-carbon; C_H1, first constant domain of the immunoglobulin heavy chain; C_L, constant domain of the immunoglobulin light chain; COM, center of mass; CVFF, consistent valence force field; Cys, cysteine; Fab, antigen-binding fragment; FLC, fluorescein; H_1, first complementarity-determining region of the heavy chain; H_2, second complementarity-determining region of the heavy chain; H_3, third complementarity-determining region of the heavy chain; His, histidine; L_3, third complementarity-determining region of the light chain; MD, molecular dynamics; MPD, 2-methyl-2,4-pentanediol; PBC, periodic boundary conditions; RDCC, residue displacement correlation coefficient; RCDM, residue displacement correlation map; RMS, root mean square; Ser, serine; Trp, tryptophan; Tyr, tyrosine; V_H, variable domain of the immunoglobulin heavy chain; V_L, variable domain of the immunoglobulin light chain; water−PBC, molecular dynamics simulations performed with full solvation and periodic boundary conditions.

0006-2960/95/0434-6962$09.00/0

binding kinetics (Kranz & Voss, 1981; Kranz *et al.*, 1981, 1982; Herron & Voss, 1983; Herron, 1984), (iii) antigen-binding thermodynamics (Herron *et al.*, 1986; Gibson *et al.*, 1988), and (iv) amino acid sequences (and genetics) (Reinitz *et al.*, 1988; Dombrink-Kurtzman *et al.*, 1989; Bedzyk *et al.*, 1989, 1990a,b). Interestingly, the kinetic studies strongly suggested that 4−4−20 undergoes a conformational change upon binding of fluorescein. Even though the three-dimensional structure of the 4−4−20 Fab−fluorescein complex was determined at 1.75 Å by X-ray diffraction (Herron *et al.*, 1989, 1994), we have been unable to crystallize the unliganded form. Thus, it has not been possible to confirm the results of the kinetic studies by comparing the structures of the unliganded and liganded forms.

With the high-resolution (1.75 Å) structure of the 4−4−20 Fab−fluorescein complex determined, we decided to use it as a starting model for parallel molecular dynamics (MD) simulations of the Fab with and without fluorescein. The results of these simulations serve as a prediction for the three-dimensional structure of the unliganded Fab. Molecular dynamics is a useful simulation method for examining the dynamic behavior of macromolecules. From simulation data, the contributions of motions at different levels (*i.e.*, side chain, secondary structure, and domain−domain interaction) can readily be examined and related to the functional role of the macromolecule. Thus, MD simulations should provide insights about the macromolecule which can both enhance and complement the experimental results. In the case of the 4−4−20 Fab, our simulations suggested that the unliganded form exhibited a greater degree of segmental flexibility than the liganded form. These simulations are discussed in detail in this paper, and the results are examined experimentally using time-resolved fluorescence spectroscopy in the following paper (Lim *et al.*, 1995).

MATERIALS AND METHODS

Molecular Models and Force Fields. The three-dimensional structure of the 4−4−20 Fab-fluorescein complex crystallized in 47% (v/v) 2-methyl-2,4-pentanediol (MPD) was used as the starting structure for MD simulations. This structure was refined to 1.75 Å resolution and contained 297 crystal water molecules (Herron *et al.*, 1994). Hydrogen atoms were added to this model using the Insight II program (BIOSYM Technologies, San Diego). Ionizable groups were protonated assuming a pH value of 7.4. The positions of the hydrogen atoms were refined by energy minimization and a short MD simulation in which the heavy atoms were held fixed and only the hydrogen atoms were allowed to move. The consistent valence force field (CVFF) (Dauber-Osguthorpe *et al.*, 1988; Burt *et al.*, 1989) was used in the potential energy calculations. BIOSYM's INSIGHT II program was used to display the molecular structures.

Preliminary Simulations. Several preliminary MD simulations of the 4−4−20 Fab were performed with the DISCOVER program (BIOSYM Technologies) as a prelude to a set of more complete simulations with full solvation and periodic boundary conditions (PBC). Initially, a simulation of the Fab−fluorescein complex in the crystal lattice was run for 120 ps. This ensemble also contained the 297 crystal water molecules mentioned above. Periodic boundary conditions were defined for the triclinic ($P1$) cell (with lattice parameters of a = 58.3 Å, b = 43.9 Å, c = 42.5 Å, α = 82.1°, β = 87.3°, and γ = 84.6°) that had been obtained for the 4−4−20 Fab−fluorescein complex crystallized in 47% MPD (Herron *et al.*, 1989, 1994). Next, separate simulations of the Fab with and without fluorescein were performed for 150 ps (Lim & Herron, 1991). In these two cases, the Fab was surrounded by a 5 Å shell of 892 water molecules. These will be referred to as "water shell simulations" because PBC were not used. This strategy was employed because our version of DISCOVER was dimensioned for 25 000 atoms, which was not large enough to accommodate the 4−4−20 Fab with full solvation and periodic boundary conditions (water−PBC). The water shell simulations convinced us that water−PBC simulations would be necessary to model the 4−4−20 Fab accurately in bulk solution, so one of us (K. Lim) wrote a new MD simulation program, which utilized the CVFF and could be dimensioned for larger ensembles.

Solvation and Periodic Boundary Conditions. In preparation for the water−PBC simulations, the Fab−fluorescein complex was solvated by placing it at the center of a solvent "box" containing water molecules that had been previously generated and energy minimized. Solvent molecules within 2.4 Å of any atom of the Fab−fluorescein complex were removed. The final molecular ensemble consisted of the Fab, fluorescein, 297 crystal water molecules, and an additional 12 023 solvent water molecules. This ensemble contained 6597 atoms for the Fab (47 782 MW), 35 atoms for fluorescein (331 MW), and 36 960 solvent atoms—which gave a total of 43 592 atoms. Initially, the density of the solvated box was slightly lower than 1.0 g/cm^3, so a low temperature (50 K) MD simulation was performed for 1 ps during which time the dimensions of the box were gradually reduced. All atoms were allowed to move during this preliminary MD simulation. The final size of the solvated box was 70.8 × 59.0 × 104.0 Å with a density of 1.03 g/cm^3. This and subsequent simulations were performed on an IBM 3090/600S supercomputer at the Utah Supercomputing Institute.

Simulations with and without Fluorescein. Two separate MD simulations were performed with the ensemble described above—one with fluorescein in the antigen-combining site and another with it removed. In the latter simulation, fluorescein was removed by applying a "pulling force" during the first 4 ps of the simulation. Specifically, fluorescein was pulled to a point outside the nonbonded cutoff distance of the Fab in increments of 0.005 Å per step using a force constant of 20 kcal/mol. Higher force constants were found to distort significantly the geometry of fluorescein. Both simulations were performed for 174 ps at 300 K with PBC and an integration step size of 10^{-15} s (1 fs). The nonbonded interaction cutoff distance was 8.5 Å with a switching function effective between 7.0 and 8.5 Å. A dielectric constant of 1.0 was used for solvated PBC ensembles. Velocity scaling was performed for the first 100 steps of each MD run, and thereafter a temperature scaling constant (0.1 ps) was used to maintain isothermal conditions. Coordinates were saved at intervals of 0.1 ps for later analysis. These coordinate sets were not energy minimized prior to analysis because of the large number of such sets (1740 for each simulation).

Analysis of Quaternary Structure. An antigen-binding fragment is composed of the entire immunoglobulin light (L) chain and a proteolytic fragment of the immunoglobulin heavy (H) chain. The light chain folds into two compact

structural units called the variable (V_L) and constant (C_L) domains, while the heavy chain fragment folds into the analogous V_H and C_H1 domains. In the Fab, the two variable domains associate to form the V_L-V_H dimer (containing the antigen-combining site), and the two constant domains associate to form the C_L-C_H1 dimer (stabilized by an interchain disulfide bond). Each domain consists of a common structural motif called the "immunoglobulin fold", which is essentially a β-barrel comprised of two antiparallel β-pleated sheets held together by a disulfide bond [see Edmundson *et al.* (1975)].

A common method for evaluating the quaternary structure of Fab fragments is to compare *pseudodyad angles* and *elbow bend angles*. A pseudodyad angle is defined for the variable (or constant) domain dimer by rotating the coordinates of the V_L (or C_L) domain around a pseudo-2-fold axis (also known as the "pseudodyad axis") into those of the V_H (or C_H1) domain. The C_α atoms of the conserved β-sheet regions are typically used for these superpositions as described by Edmundson *et al.* (1975). The elbow bend angle is determined by computing the angle between the variable and constant pseudodyad axes.

In addition to pseudodyad and elbow bend angles, a somewhat different approach was also employed to assess the dynamical changes in quaternary structure that occurred within the Fab during the course of MD simulations. Using again the C_α coordinates of the conserved β-sheets, two new parameters were defined—*plane angles* and *axis angles*. For calculation of plane angles, a plane is first defined between the two β-sheets of each domain, approximately parallel to both, and then the dihedral angle formed between two such planes is determined. In the case of axis angles, an axis is defined for each domain that is parallel to the above plane and runs in the direction of the long dimension of individual domains. An axis angle is formed between two such domain axes. Plane and axis angles can be computed for any pair of domains in the Fab, though only V_L-V_H, C_L-C_H1, V_L-C_L, and V_H-C_H1 will be used in this paper.

RESULTS

Crystal Lattice Simulation. The crystal lattice simulation was performed for 120 ps. Each coordinate set, saved at 0.1 ps intervals, was superimposed onto the X-ray structure using a least squares fitting algorithm. During the first 40 ps, the RMS deviation of all main-chain atoms (N, C_α, and C) from the X-ray structure increased to *ca.* 2.5 Å but then remained constant for the next 80 ps. The average RMS deviation during the 80 ps period was 2.51 ± 0.05 Å. The small standard deviation of this number indicated that the simulation had probably reached equilibrium after the first 40 ps. The observed RMS deviation between the MD simulation and the X-ray structure was probably due to inherent differences between the force fields and energy calculation algorithms used in the two methods. As mentioned previously, the crystal lattice simulation was performed with BIOSYM's DISCOVER program, while the X-ray structure was refined using X-PLOR (Brünger, 1991). In the latter, an extra term is added to the potential energy expression that is derived from the mean square deviation between the observed and calculated structure factors. Thus, a structure minimized with X-PLOR has to conform both to the force field and to the experimentally obtained diffraction data. Another difference between the X-ray and MD structures was that a variant of the CHARMm force field (Brooks *et al.*, 1983) was used in the former, while BIOSYM's CVFF (Dauber-Osguthorpe *et al.*, 1988; Burt *et al.*, 1989) was used in the latter.

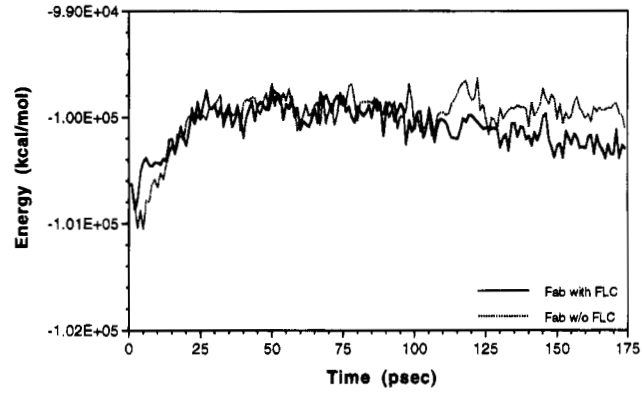

FIGURE 1: Potential energy profile of molecular dynamics (MD) simulations of the 4−4−20 Fab with full solvation and periodic boundary conditions (water-PBC): solid line, Fab with fluorescein (FLC); dashed line, Fab without fluorescein.

In order to determine whether or not the quaternary structure of the Fab changed significantly during the crystal lattice simulation, average RMS deviation values (relative to the X-ray structure) were calculated for main-chain atoms in the variable domain dimer and the constant domain dimer. As mentioned previously, the angle formed by these two dimers is known as the "elbow bend angle" and is known to vary in different Fab structures (Sheriff *et al.*, 1988). Average RMS deviation values of 2.38 ± 0.07 and 2.46 ± 0.07 Å were determined for main-chain atoms in the variable and constant dimers, respectively. The fact that these values were very similar to that obtained for the whole Fab (2.51 Å) suggested that the quaternary structure did not change significantly during the crystal lattice simulation.

General Features of the Water−PBC Simulations. The water−PBC simulations were performed for 174 ps. Figure 1 shows potential energy plots for the Fab with and without fluorescein over this period. Inspection of these plots showed that both simulations reached equilibrium after *ca.* 24 ps. For the remainder of the simulations (24−174 ps), the potential energy of the ensemble with fluorescein in the antigen-combining site was slightly lower (*ca.* 200 kcal/mol) than that of the ensemble with fluorescein removed. Examination of potential energies computed from the last 50 ps of the simulations suggested that the above energy difference arose primarily from different electrostatic interactions between the bound and free forms (Table 1). The electrostatic interaction between the V_L domain and water was 184 kcal/mol lower (more favorable) in the bound form than in the unbound form. This was partially offset by the electrostatic interaction between fluorescein and water, which was 100 kcal/mol higher (less favorable) in the bound form. Moreover, significant differences were observed in intradomain electrostatic interactions between the bound and free forms. In particular, the electrostatic energy of the V_L domain was 115 kcal/mol higher in the bound form, while that of the C_L domain was 338 kcal/mol lower in the bound form. Taken together, these results suggest that the binding of the dianionic fluorescein molecule produced major changes in the electrostatic character of both the V_L and C_L domains. Although this energy change was not surprising

Table 1: Electrostatic Potential Energies from Water−PBC Simulations[a]

	(I) Fab with Fluorescein					
	V_L	C_L	V_H	C_H1	FLC[b]	H_2O
V_L	−60.3 ± 42.8	−34.2 ± 34.4	−155.2 ± 17.0	0.0	−109.8 ± 7.1	−1860.7 ± 72.0
C_L		−379.5 ± 44.4	0.0	−111.6 ± 23.3	0.0	−2266.0 ± 79.8
V_H			−560.4 ± 64.5	2.8 ± 3.8	−10.5 ± 13.5	−2211.7 ± 95.3
C_H1				1076.0 ± 33.5	0.0	−1689.4 ± 50.9
FLC[b]					20.3 ± 1.5	−120.6 ± 11.0
H_2O						−134664.9 ± 350.9
	(II) Fab without Fluorescein					
	V_L	C_L	V_H	C_H1	FLC	H_2O
V_L	−175.3 ± 57.1	6.0 ± 16.4	−207.6 ± 20.9	0.0	−0.2 ± 1.8	−1676.9 ± 64.2
C_L		−41.8 ± 61.3	−0.1 ± 0.3	−113.0 ± 24.5	0.0	−2480.2 ± 80.0
V_H			−557.4 ± 57.1	−5.3 ± 4.7	5.9 ± 10.2	−2267.5 ± 77.8
C_H1				1071.8 ± 31.4	0.0	−1654.6 ± 60.4
FLC[b]					19.5 ± 2.2	−220.6 ± 15.4
H_2O						−134531.0 ± 318.1

[a] Molecular dynamics simulations were performed over a period of 174 ps. During the last 50 ps of the simulation (124−174 ps) the electrostatic potential energy was computed at intervals of 0.1 ps for several different pairwise interactions (*e.g.*, V_L domain with the V_H domain). These values were averaged and reported in this table along with their standard errors. All values are in units of kcal mol^{-1}. [b] FLC: fluorescein.

in the case of the V_L domain, where Arg 39L[2] makes a salt link with fluorescein, it was unexpected to find changes in the C_L domain as well.

Comparison of the water−PBC simulation structures with the X-ray structure indicated changes within the Fab. The RMS difference between the simulated and X-ray structures increased gradually during the course of the simulation (Figure 2a). By the end of the 174 ps simulation period, an RMS difference of *ca.* 3.2 Å was observed for the Fab with bound fluorescein and a value of *ca.* 3.5 Å for the Fab without fluorescein. In contrast, smaller RMS differences were observed when the main-chain atoms of the variable domain dimer alone or constant domain dimer alone were superimposed (Figure 2b,c). This suggested that the orientation of the two domain dimers, with respect to each other, had changed from the original X-ray structure (see section on quaternary structure analysis below). Because the two domain dimers are only linked to each other by two extended peptide regions (switch peptides), they should exhibit greater flexibility during a simulation in a large water box than when constrained in a crystal environment.

Analysis of the Antigen-Combining Site. Seven contact residues (defined in Figure 3a) were used to analyze the geometry of the antigen-combining site. Lines were drawn between the centers of mass of the amino acid side chains to define the volume of the site and several internal angles (see Figure 3b and Table 2). Both of these parameters were examined during the course of the MD simulations (Figure 4, Table 2). This analysis revealed that the volume of the combining site of the Fab with fluorescein remained relatively constant throughout the 174 ps simulation. In contrast, when fluorescein was initially removed from the Fab, the volume of the antigen-combining site decreased precipitously during the first 10 ps of the simulation but then gradually returned to its original volume—reaching a new equilibrium at about 120 ps (Figure 4).

[2] The strict sequential numbering system used in our computer graphics workstations is employed throughout this paper. This numbering scheme is consistent with the coordinates for the structure of the 4−4−20 Fab crystallized in MPD, which have been deposited in the Protein Data Bank (4FAB). A comparison between this strict sequential scheme and the general numbering scheme introduced for immunoglobulins by Kabat *et al.* (1991) is presented elsewhere (Herron *et al.*, 1994).

Of the three internal angles defined in Table 2, only one (Trp 101L−Arg 39L−Tyr 103H) varied significantly between the two simulations. Specifically, the value observed for the Fab without fluorescein (*ca.* 70°) was about 30° more acute than the value observed for the Fab with fluorescein (*ca.* 100°) (Table 2). In another comparison, the above seven combining site residues in the MD structures were superimposed on their counterparts in the X-ray structure, and the RMS deviation was computed at 0.1 ps intervals for all non-hydrogen atoms. These data were averaged over the period of 24−174 ps. Average RMS deviation values of 1.19 ± 0.12 and 1.72 ± 0.14 Å were computed for the Fab with fluorescein and without fluorescein, respectively. Taken together, these results suggest that the conformation of the antigen-combining site is not stable in the absence of fluorescein and that the above residues rearrange themselves into a more stable conformation.

In Figure 5, side-by-side comparisons of antigen-combining sites with and without fluorescein are shown at four different time points in the MD trajectory (10, 20, 70, and 170 ps). These times were chosen to show the conformation of the site at various points during the volume recovery process. For the Fab with fluorescein (Figure 5, left column), the amino acid residues remained in place during the course of the simulation due to their close interactions with fluorescein. Only His 31L, located at the mouth of the binding site, exhibited a relatively large degree of motion. For the Fab without fluorescein (Figure 5, right column), the initial collapse was caused by a movement of the side chains of many of the aromatic contact residues (Tyr 37L, Trp 101L, Trp 33H, Tyr 103H) into the space previously occupied by fluorescein (Figure 5, 10 ps view). Most of these side chains moved away from the center of the site over the next 70 ps of the simulation, thus helping to restore its volume (Figure 5, 20 and 70 ps views). By the end of the simulation, the two tyrosines had returned close to their original positions, but the two tryptophans occupied new positions (Figure 5, 170 ps). Specifically, Trp 33H was located further from the center of the combining site than in the Fab with fluorescein, while Trp 101L was located in a part of the site normally occupied by the xanthenone ring of fluorescein.

The volume recovery of the antigen-combining site also proceeded with the influx of water molecules. In Figure 6,

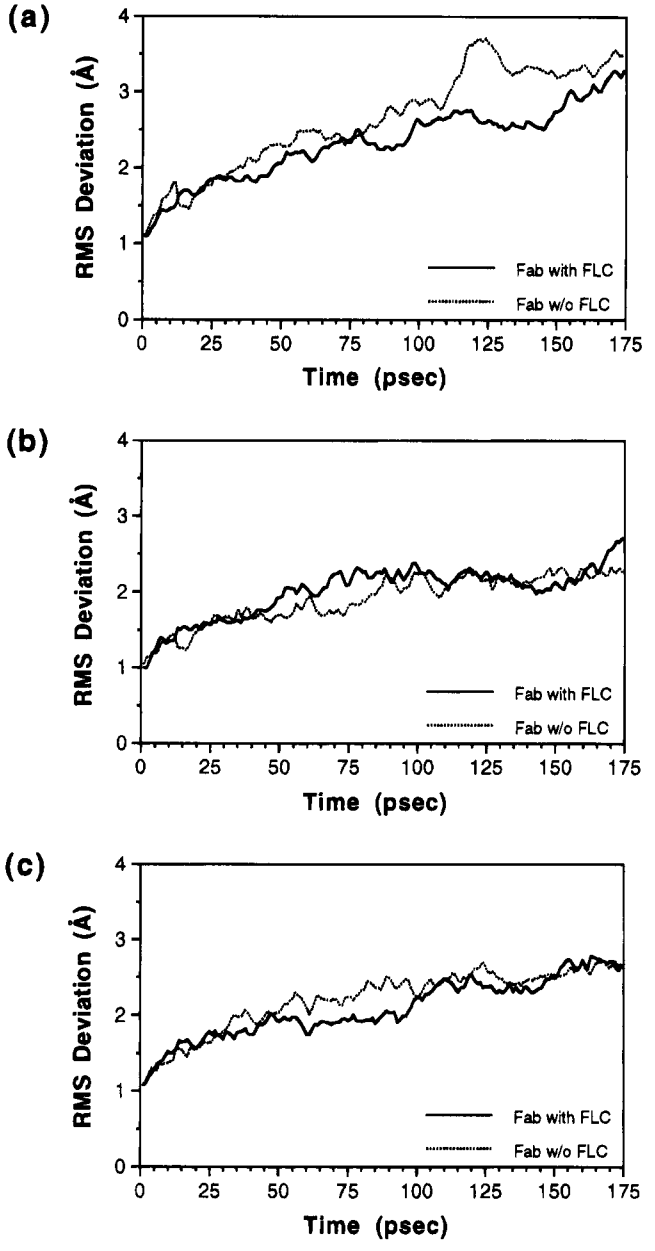

FIGURE 2: Comparison of simulated and X-ray structures. Coordinates were saved at 0.1 ps intervals during water–PBC simulations, and main-chain atoms (N, C_α, and C) were superimposed on their counterparts in the 1.75 Å X-ray structure of the 4–4–20 Fab–fluorescein complex (Herron *et al.*, 1994). The RMS deviation of main-chain atoms was plotted versus the simulation time scale (0–174 ps). The following three comparisons were performed: (a) entire Fab, (b) variable domain dimer (V_L–V_H), and (c) constant domain dimer (C_L–C_H1). Plots: solid line, Fab with fluorescein (FLC); dashed line, Fab without fluorescein.

the combining site of the Fab without fluorescein is shown in two different views. For sake of clarity, CPK models were used to illustrate the water molecules. The presence of a continuous line of water molecules from the outside of the combining site into the interior suggests that their role is to stabilize the site in the absence of antigen. For example, two water molecules (shown in green and light blue) located in the interior of the site helped stabilize Arg 39L and Asp 106H (buried deep in the interior of the site) in the absence of fluorescein. Interestingly, both of these water molecules were derived from the X-ray structure and remained fixed in their original positions throughout the MD simulation.

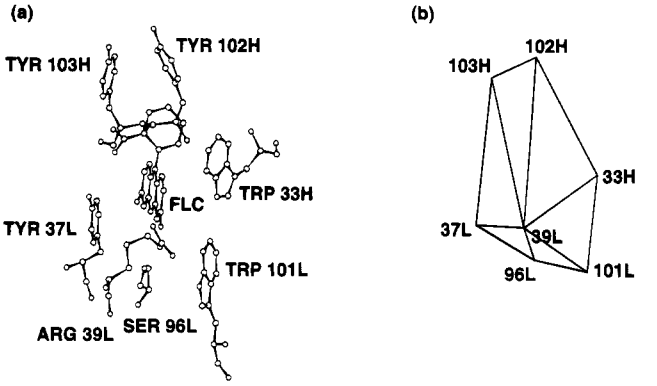

FIGURE 3: Geometry of the antigen-combining site: (a) ball-and-stick model; (b) lines drawn between the centers of mass of amino acid side chains. The volume was calculated from the sum of four tetrahedrons defined using the following sets of residues as vertices: 39L–96L–101L–33H, 37L–39L–96L–33H, 39L–33H–102H–103H, and 37L–39L–33H–103H.

Conformation of Fluorescein. Fluorescein consists of a three-ring xanthenone group coupled to a phenyl carboxylate group. When a force constant value of 163 kcal mol^{-1} $Å^{-2}$ (originally assigned by the CVFF) was used for the carbon–carbon bond connecting the two ring groups, the atoms in the xanthenone ring were pulled toward this bond, thus distorting the ring shape. Reduction of this value to 120 kcal mol^{-1} $Å^{-2}$ prevented such distortion. Smaller values had the unwanted effect of lengthening the bond.

The planarity of the xanthenone ring was measured with an angle formed by two halves of the ring. The dihedral angle between the xanthenone and phenyl rings was also calculated. For fluorescein in the antigen-combining site, the average values computed from the MD simulations (24–174 ps) were 174.2 ± 3.7° for ring planarity and 114.4 ± 6.1° for the dihedral angle. (For comparison, corresponding values were 178.8° and 110.6° for fluorescein in the original X-ray structure.) When fluorescein was removed from the combining site, the corresponding values were 171.2 ± 9.2° and 117.2 ± 6.2°. Thus, neither the dihedral angle nor ring planarity varied significantly between the two simulations.

Analysis of Quaternary Structural Changes in the Fab. Although the tertiary structures of the four individual domains remained intact during the MD simulations, the quaternary structure of the Fab fluctuated significantly. In the crystal lattice simulation, the pseudodyad and elbow bend angles were computed at intervals of 0.1 ps over the period of 40–120 ps. These measurements were averaged and gave values of 172.9 ± 1.6° for the pseudodyad angle of the variable domain dimer, 166.9 ± 1.3° for the pseudodyad angle of the constant domain dimer, and 173.3 ± 0.9° for the elbow bend angle, whereas comparable values of 176.3°, 171.4°, and 173.6° were determined for these three angles from the X-ray structure (Table 3). These results suggested that all three angles were strongly restrained by crystal packing interactions.

Pseudodyad and elbow bend angles were computed for water–PBC simulations at 0.1 ps intervals over the period of 24–174 ps. In this case, however, fluctuations were somewhat greater than observed in the crystal lattice simulation (Table 3). This was especially true in the case of the Fab without fluorescein where the pseudodyad angle of the variable domain dimer decreased by more than 10° from that of the X-ray structure. In addition, the removal of fluorescein

Table 2: Geometry of the 4−4−20 Antigen-Combining Site during the Course of Water−PBC Simulations[a]

	internal angle (deg)					
	Fab with fluorescein			Fab without fluorescein		
	24−74 ps	74−124 ps	124−174 ps	24−74 ps	74−124 ps	124−174 ps
Tyr 37L−Arg 39L−Tyr 102H	57.2 ± 1.7	55.9 ± 2.1	57.5 ± 2.6	58.7 ± 3.6	62.4 ± 6.4	56.8 ± 4.8
Ser 96L−Arg 39L−Tyr 102H	94.3 ± 4.1	92.0 ± 2.7	92.5 ± 2.8	89.4 ± 5.5	87.4 ± 6.0	87.9 ± 3.9
Trp 101L−Arg 39L−Tyr 103H	97.5 ± 4.3	102.0 ± 4.3	102.7 ± 6.1	70.0 ± 5.0	75.7 ± 5.4	69.9 ± 4.2

[a] Combining site geometry was analyzed by drawing lines between the centers of mass of Arg 39L and five other key contact residues (see Figure 3b). These lines were used to define three different internal angles in the combining site, all with Arg 39L at the vertex. Values for these angles were computed at intervals of 0.1 ps over a period of 24−174 ps. These data were reduced by computing the average and standard error of each angle over three 50 ps periods (24−74, 74−124, and 124−174 ps).

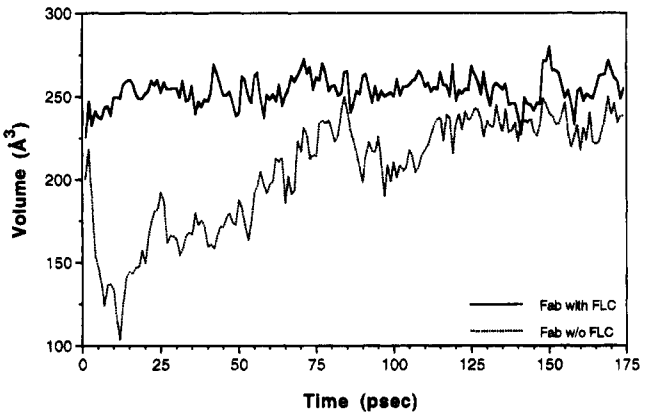

FIGURE 4: Changes in the volume of the antigen-combining site during the course of water−PBC simulations: solid line, Fab with fluorescein (FLC); dashed line, Fab without fluorescein.

from the binding site caused the elbow bend angle to decrease, and after 125 ps, it stabilized at *ca.* 158°. In contrast, the elbow bend angle for the Fab with fluorescein fluctuated about its value in the X-ray structure throughout the course of the simulation (see Table 3).

Axis and plane angles were also calculated at 0.1 ps intervals during the course of the water−PBC simulations, and these values were averaged over intervals of 50 ps, starting after the initial 24 ps equilibration period (24−74, 74−124, and 124−174 ps; see Table 3). For the Fab with fluorescein the mean values of both the V_L−V_H and the C_L−C_H1 axis angles decreased by *ca.* 6° each during the course of the simulation. Such changes reflect a scissors-like motion of the V_L domain relative to V_H and also of the C_L domain relative to C_H1. The scissor motion is probably an intrinsic fluctuation of the Fab, rather than a ligand-induced effect, because similar changes were observed in the Fab without fluorescein. In contrast, the intrachain axis angles (V_L−C_L and V_H−C_H1) became more acute for the Fab without fluorescein, which reflected the change in the elbow bend angle of the unliganded species. The plane angles also exhibited differences between the Fab with and without fluorescein, but these angles are best viewed as phenomenological indicators of fluctuations in quaternary structure because they reflect complex motions consisting of rotations around at least two of a domain's ellipsoidal axes.

Comparison of the MD structures of the Fab with and without fluorescein indicated that significant differences in the domain positions had occurred (Figures 7 and 8). The computer animation revealed that the movements of these structures involved the cooperative motion of numerous elements of the Fab structure. As mentioned previously, in the Fab without fluorescein the side chain of Trp 101L moved to partially fill the void left by fluorescein. This movement was actually part of the overall movement of the rest of the β-strand to which Trp 101L was attached (101L−109L). As a result, the adjacent switch region peptide (110L−114L) moved toward the V_L domain, which in turn affected the conformation of the C_L domain. In the Fab with fluorescein, a loop region in C_L (173L−177L) was closely associated with the switch region peptide (110L−114L). However, in the absence of fluorescein, this switch region was pulled toward the V_L, and its interaction with the 173L−177L loop was broken. When this happened, the greater freedom of movement of the 173L−177L loop caused a change in the rest of the C_L such that the whole domain was seen to roll or rotate about its long axis. Compared to the X-ray structure and the Fab with fluorescein (Figure 7), the relative positions of the V_L and V_H deviated greatly for the Fab without fluorescein (Figure 8).

Structural changes also occurred in the heavy chain. In the initial stage of the MD simulation (when fluorescein was pulled out of the binding site) the first and second complementarity-determining regions (H_1, 31H−34H; H_2, 50H−68H) collapsed toward the binding site. When this happened, the adjacent 76H−79H loop moved in such a way to allow the V_H domain to more closely approach the C_H domain. The distance between the switch region (117H−120H) and a loop region in the C_H1 (176H−179H) was shortened by about 2 Å. This change may have also been affected by the changes in the C_L region described above. Thus, these movements influence the angular relationships between the four domains of the Fab and led to the observed changes in the elbow bend angle.

Residue Displacement Correlation Maps. Although quaternary structure parameters such as elbow bend, plane, and axis angles gave indications of Fab domain movements, a more detailed analysis of structural changes can be obtained from cross-correlation functions. Such functions can reveal concerted atomic motions and help to distinguish the differences between the Fab with and without bound fluorescein. The cross-correlation coefficient between any two atoms is expressed as

$$C_{ij} = \frac{\langle \Delta r_i \cdot \Delta r_j \rangle}{\sqrt{\langle \Delta r_i \rangle^2 \langle \Delta r_j \rangle^2}} \quad (1)$$

where Δr is the displacement vector from the mean position of the ith atom and angle brackets indicate the time average (Ichiye & Karplus, 1991; Harte *et al.*, 1992). The value of C_{ij} can range from +1 to −1, correlated and anticorrelated, respectively. Complete correlation may be interpreted as motions having the same phase as well as the same period

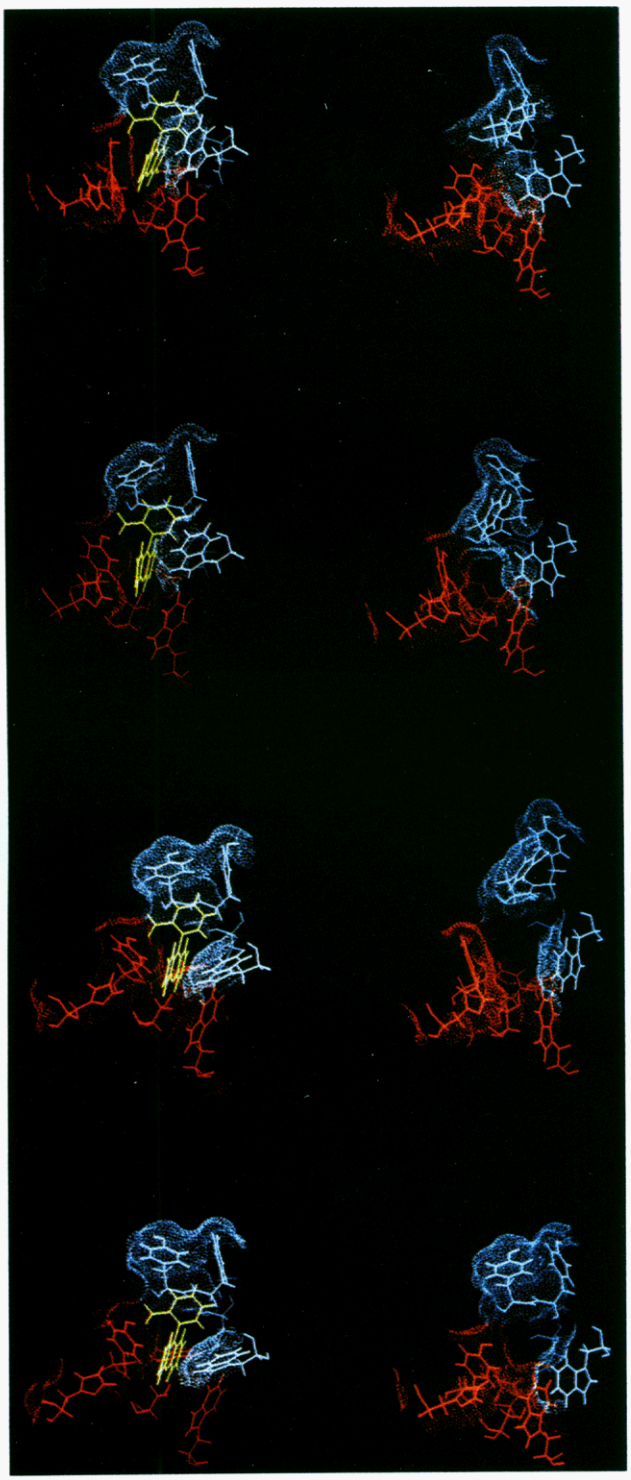

FIGURE 5: Changes in the conformation of the antigen-combining site for the Fab with fluorescein (left column) and without fluorescein (right column) during water−PBC simulations at 10 ps (first or top row), 20 ps (second row), 70 ps (third row), and 170 ps (fourth row). Light chain contact residues are colored red; heavy chain contact residues are colored blue; and fluorescein is colored green. The combining site is oriented so that the viewer is looking directly into the mouth of the binding cavity. The stereochemistry of each of the four structures was optimized by simulated annealing from 300 to 50 K.

and anticorrelation as motions having the same period but with displacements out of phase at an angle of 180°. When C_{ij} is close to 0, the motions of i and j deviate from a straight line and become random with respect to each other.

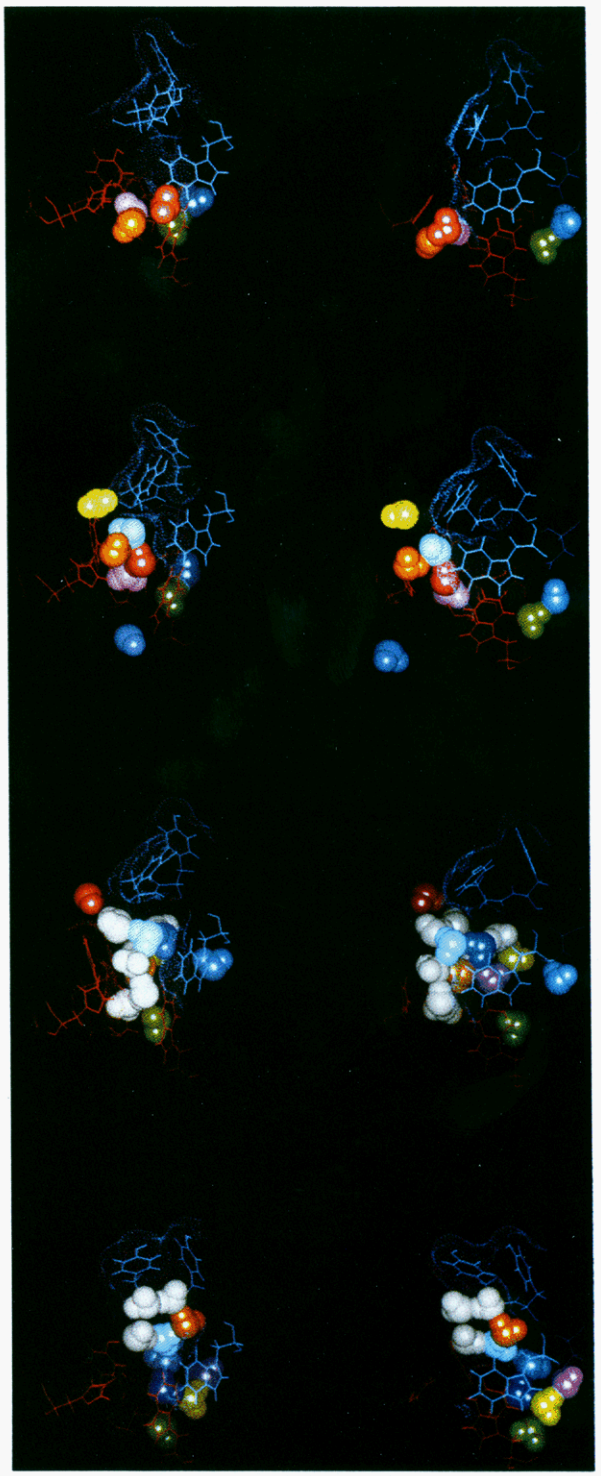

FIGURE 6: Solvation of the antigen-combining site for the Fab without fluorescein at 10 ps (first or top row), 20 ps (second row), 70 ps (third row), and 170 ps (fourth row). Two different views are shown. The images in the left column are identical to those shown in the right column of Figure 5, except that solid CPK models of solvent molecules are also included. The images in the right column were generated by rotating those in the left column by 90° around the Z-axis (vertical axis) of the laboratory axes system. In this view, the mouth of the combining site opens to the left. Solvent molecules colored green, light blue, violet, and orange were derived from the X-ray structures, while others were added for water−PBC simulations. Solvent molecules colored white were more transitory (or dynamic) than their colored counterparts. The stereochemistry of each of the four structures was optimized by simulated annealing from 300 to 50 K.

Table 3: Quaternary Structure of the 4−4−20 Fab during the Course of Water−PBC Simulations[a]

parameter	X-ray Fab[b]	Fab with fluorescein			Fab without fluorescein		
		24−74 ps	74−124 ps	124−174 ps	24−74 ps	74−124 ps	124−174 ps
variable domain pseudodyad	176.3	168.1 ± 3.3	168.7± 1.3	170.0 ± 2.6	166.7 ± 1.2	164.9 ± 2.0	163.6 ± 1.7
constant domain pseudodyad	171.4	166.8 ± 1.8	167.8 ± 2.4	171.4 ± 3.9	170.0 ± 1.7	173.4 ± 1.6	174.6 ± 1.5
elbow bend angle	173.6	174.1 ± 1.0	173.0 ± 3.1	173.7 ± 1.8	170.5 ± 1.7	165.1 ± 5.0	158.2 ± 1.5
axis angles							
V_L-V_H	77.1	73.0 ± 1.9	70.0 ± 1.7	66.6 ± 2.1	76.4 ± 1.7	74.9 ± 4.4	68.3 ± 1.8
V_L-C_L	89.0	89.4 ± 2.0	89.2 ± 2.1	96.6 ± 3.9	87.5 ± 1.5	86.9 ± 2.3	86.7 ± 1.5
C_L-C_H1	93.8	109.0 ± 2.0	104.2 ± 2.5	101.8 ± 3.0	107.0 ± 1.8	105.9 ± 1.7	103.5 ± 2.0
V_H-C_H1	117.5	106.1 ± 1.6	108.8 ± 4.5	111.5 ± 2.6	112.7 ± 3.6	118.4 ± 4.8	121.0 ± 2.6
plane angles							
V_L-V_H	39.8	37.2 ± 1.7	40.8 ± 2.2	37.3 ± 1.7	34.6 ± 3.8	30.6 ± 2.2	31.0 ± 2.1
V_L-C_L	120.7	123.3 ± 3.1	127.2 ± 2.4	116.7 ± 3.8	123.8 ± 3.1	121.3 ± 1.7	124.8 ± 2.4
C_L-C_H1	44.0	34.5 ± 2.9	33.5 ± 3.2	32.5 ± 3.4	29.7 ± 2.4	25.1 ± 1.9	23.9 ± 2.5
V_H-C_H1	92.3	99.0 ± 2.7	102.4 ± 2.6	100.2 ± 1.9	97.6 ± 2.7	98.5 ± 2.4	97.7 ± 2.4

[a] Angle values for various quaternary structural parameters were computed at intervals of 0.1 ps over a period of 24−174 ps. [b] The X-ray structure of the Fab−fluorescein complex (1.75 Å resolution) crystallized in 47% (v/v) 2-methyl-2,4-pentanediol (Herron *et al.*, 1994).

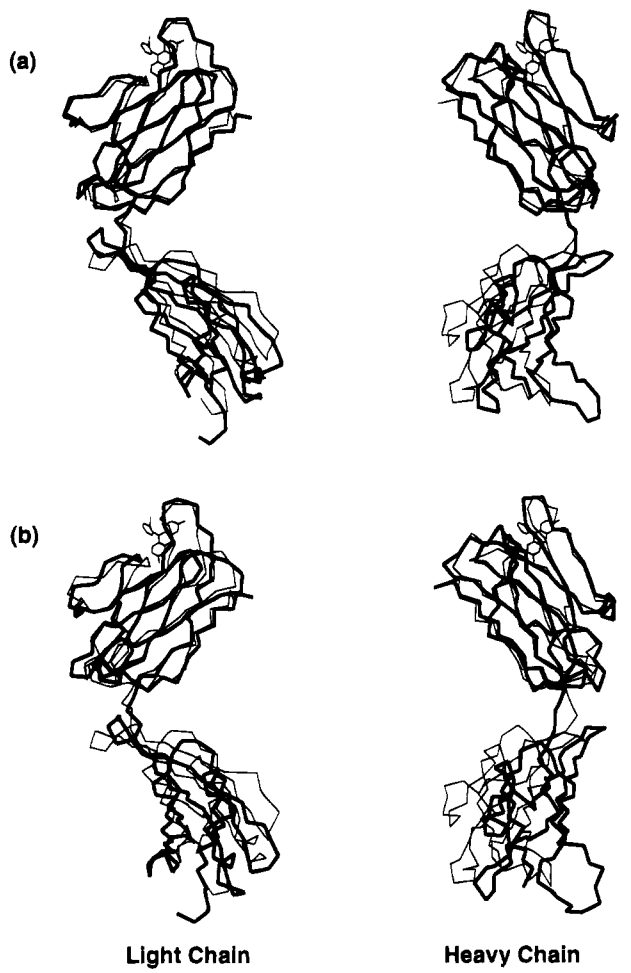

FIGURE 7: Comparison of the C_α trace of the Fab with fluorescein from the water−PBC simulations (thick lines) to that of the X-ray structure (thin lines) (a) at 70 ps and (b) at 170 ps. Light chains (shown on the left) were superimposed using C_α atoms from the V_L domain, while heavy chains (shown on the right) were superimposed using C_α atoms from the V_H domain. The two chains are separated for clarity.

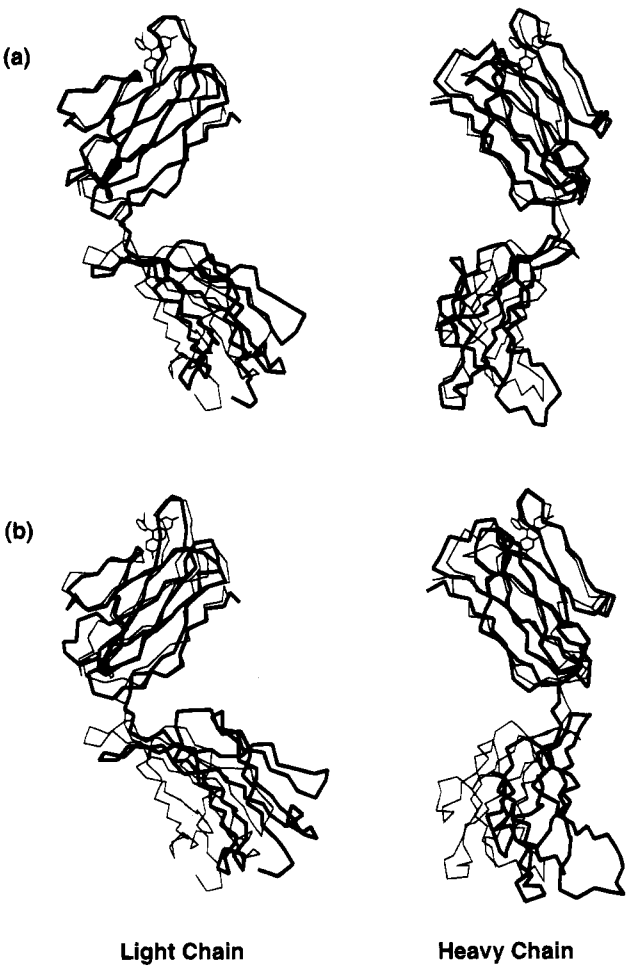

FIGURE 8: Same as in Figure 7 but for the Fab without fluorescein.

Molecular dynamics trajectories of the Fab both with and without fluorescein were analyzed over the period of 50−174 ps using cross-correlation functions. Displacement vectors were computed as follows: (i) the center of mass (COM) of the main-chain atoms in each amino acid residue was computed for each time interval in the 124 ps period, (ii) these values were then used to determine the average COM for each residue over the 124 ps period, and (iii) the displacement of the COM of each residue from its average position was computed for each time interval. (The center of mass was used rather than individual atoms to simplify the presentation of data.) The following three cross-correlations were performed: (i) light chain residues with light chain residues, (ii) heavy chain residues with heavy chain residues, and (iii) light chain residues with heavy chain residues. These data were presented as a series of contour plots called residue displacement correlation maps (RDCM) in Figures 9 and 10.

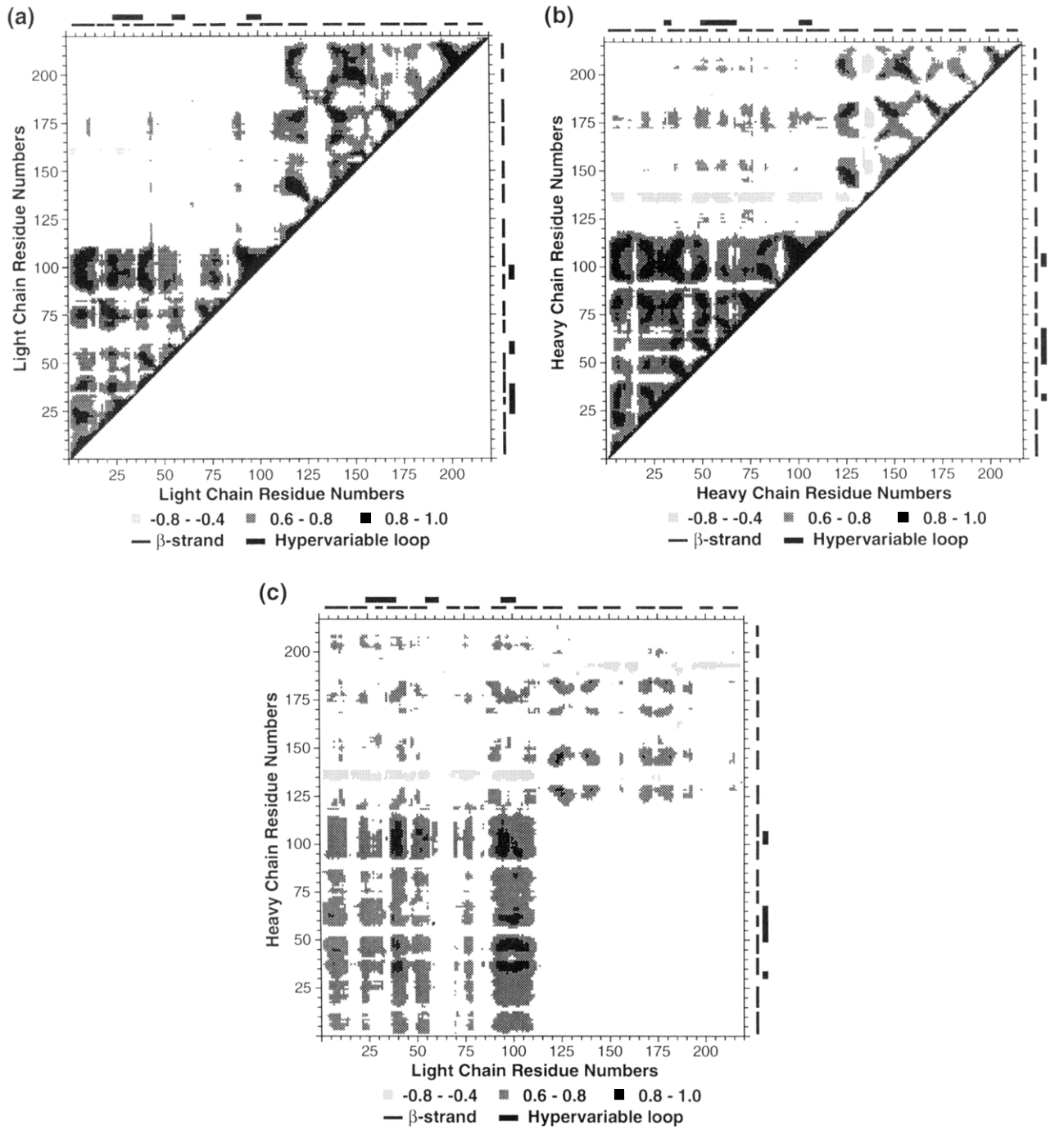

FIGURE 9: Residue displacement correlation maps (RDCM) for the Fab with fluorescein: (a) light chain−light chain interactions; (b) heavy chain−heavy chain interactions; (c) light chain−heavy chain interactions. Thin bars at the top and right side of each graph denote β-sheet regions and thick bars the complementarity-determining regions (CDRs). Correlation coefficients were calculated as described in the text. Plotted values were averaged over the final 124 ps of the simulation (50−174 ps).

In general, residue displacement correlation coefficient (RDCC) values observed between residues of the conserved β-sheet regions in each domain were higher than those in the loops and turns. The same was true for residues located at the interface of the light and heavy chains. Most of the RDCC values were positive, but some significant negative RDCC values were also observed. For the Fab with fluorescein, the 130H−140H loop in the C_H1 domain exhibited negative correlation with many other residues (Figure 9b,c). This loop is located at the opposite end of the Fab from the binding site and contains Cys 133H which forms the interchain disulfide bond with Cys 219L in the light chain. Correlations within each domain were relatively higher than those between domains, especially for the variable domains. For the Fab with fluorescein, the C_H1 domain contributed more to the correlations of interdomain residues than other domains (Figure 9b,c).

A greater degree of correlation was observed for the Fab with fluorescein than for the Fab without fluorescein. Of particular note was the strong correlation between the V_L and V_H domains, an effect which largely disappeared in the Fab without fluorescein (Figures 9c and 10c). Cross-correlation calculations were also performed for shorter time intervals (10, 30, and 60 ps) (data not shown). These calculations showed that the above strong positive correlations only became evident at intervals of 60 ps and larger.

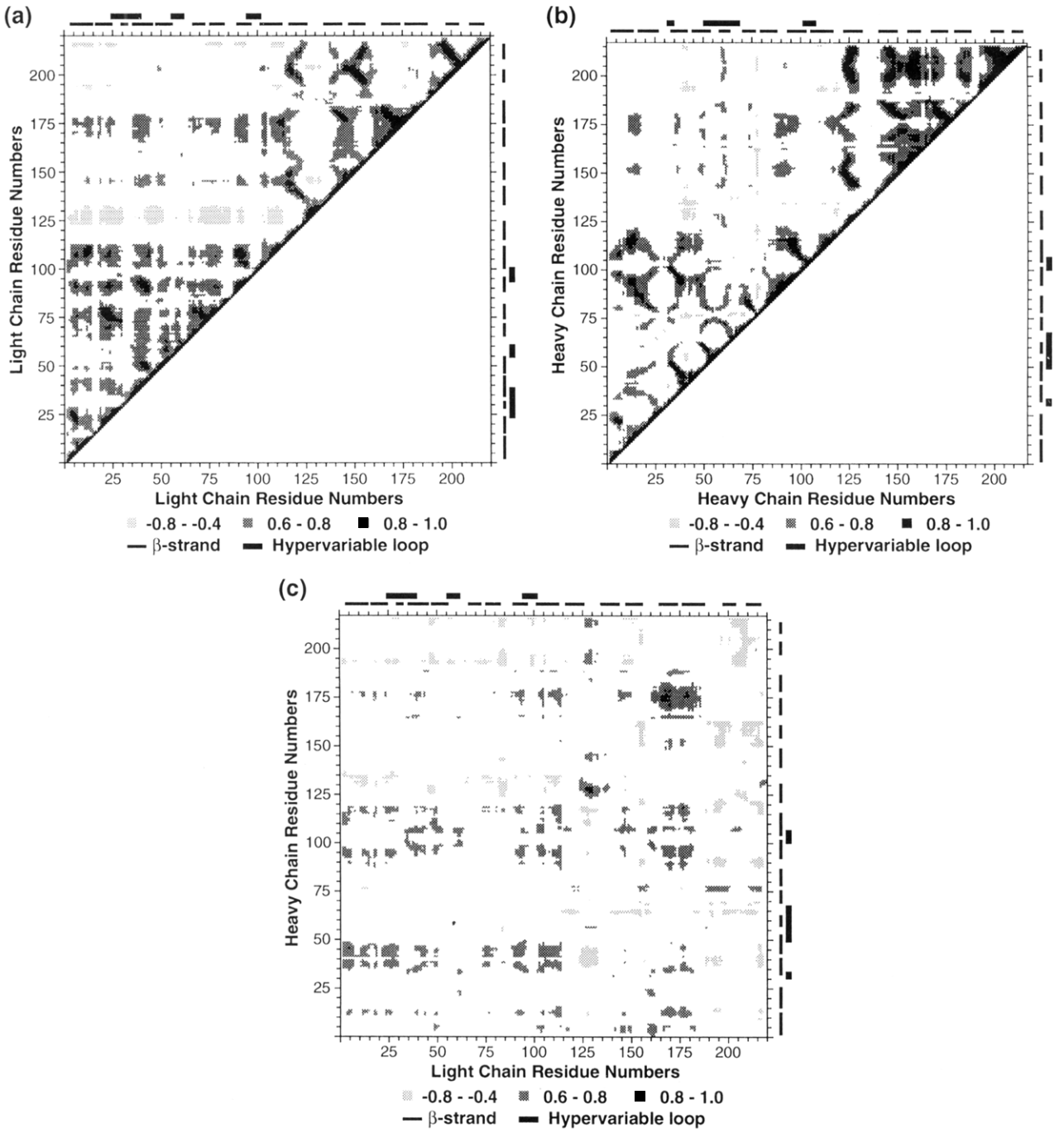

FIGURE 10: Same as in Figure 9 but for the Fab without fluorescein.

The removal of antigen also resulted in a smaller and more equal distribution of correlations among the residues; this was observed for all four domains. In addition, a higher number of negative correlations were observed for the Fab without fluorescein. Finally, correlations between bound fluorescein and residues of the Fab are shown in Figure 11. Fluorescein's correlations with the complementarity-determining regions were characteristically high.

Correlation to Time-Resolved Fluorescence Experiments. Considering the number of assumptions and approximations that are inherent to MD simulations, it is often useful to cross-correlate results obtained from simulation studies to those obtained experimentally. Most of our preceding discussion dealt with either the local motion of residues that comprise the antigen-combining site or the segmental motion of the Fab's four domains. While few if any experimental techniques can provide detailed information about picosecond motions of individual residues for a protein the size of a Fab fragment (50 000 MW), the segmental motion of immunoglobulin domains can been studied using fluorescence polarization (Yguerabide *et al.*, 1970; Oi *et al.*, 1983; Hanson *et al.*, 1981, 1985). In this technique, a fluorescent label is conjugated to the protein, and its fluorescence is excited with plane polarized light. The fluorescence emission is also polarized, and the degree of polarization (also called anisotropy) is related to the angle between the excitation and emission dipoles of the label:

$$r = \frac{2}{5}\left(\frac{3\cos^2\alpha - 1}{2}\right) \qquad (2)$$

where r is the steady-state fluorescence anisotropy and α

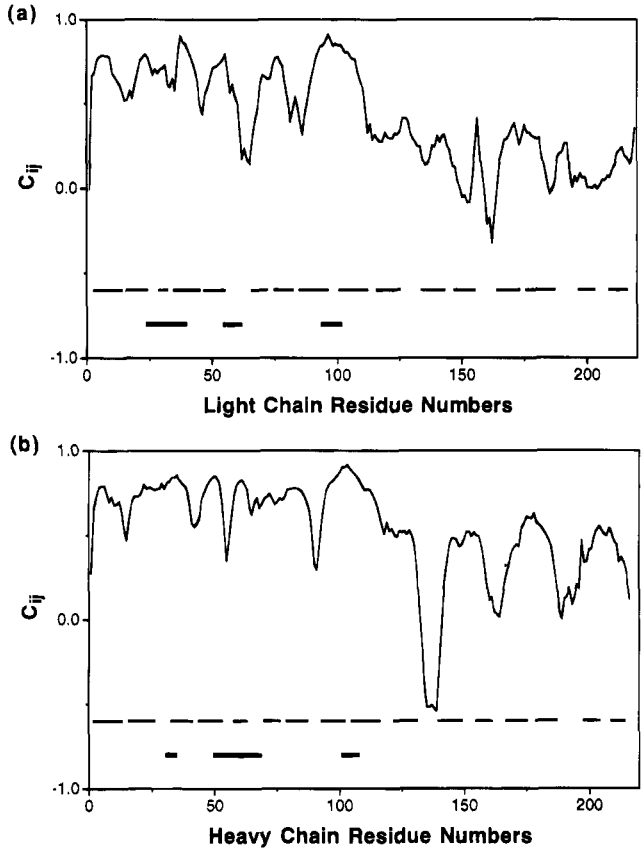

FIGURE 11: Cross-correlation between bound fluorescein and Fab residues during the period of 50−174 ps: (a) fluorescein−light chain interaction and (b) fluorescein−heavy chain interaction. Thin bars at the bottom of each graph denote β-sheet regions and thick bars the complementarity-determining regions (CDRs). Main-chain atoms (N, C_α, and C) were used for each Fab residue and all non-hydrogen atoms for fluorescein.

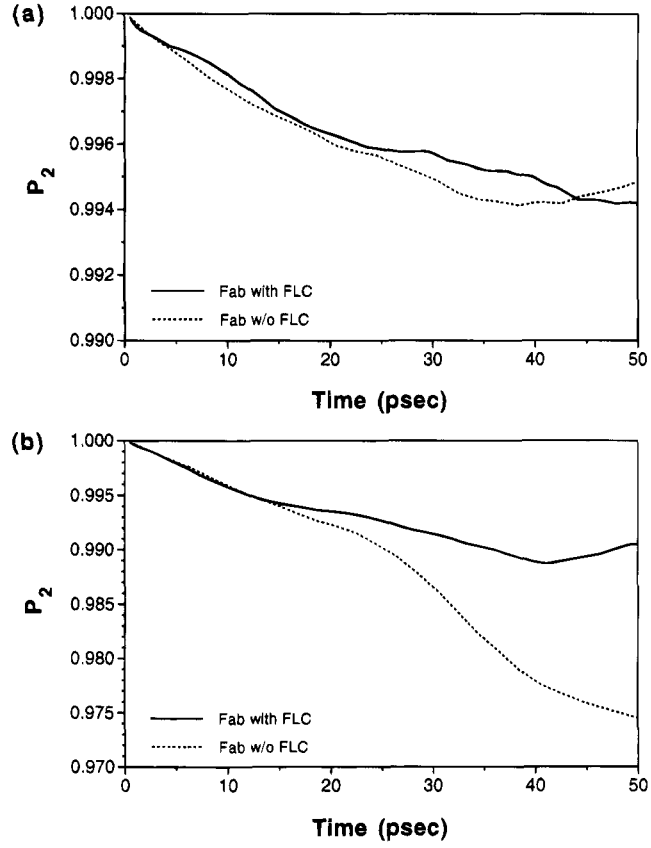

FIGURE 12: Decay function of the pseudo-2-fold axis of (a) the variable domain dimer and (b) the constant domain dimer from water−PBC simulations: solid line, Fab with fluorescein (FLC); dashed line, Fab without fluorescein.

the angle between the excitation and emission dipoles.

This angle can also be affected by the global and segmental motion of the Fab, in which case $\cos^2 \alpha$ can be expressed in the time domain as the dot product of the normalized vectors $\hat{\mu}_a(t)$ for absorption (or excitation) and $\hat{\mu}_e(t)$ for emission:

$$r(t_m) = \frac{2}{5(N-m)} \sum_{n=1}^{N-m} P_2[\hat{\mu}_a(t_n) \cdot \hat{\mu}_e(t_n + t_m)] \qquad (3)$$

where $P_2[\hat{\mu}_a \cdot \hat{\mu}_e]$ is a second-order Legendre polynomial, N the number of data sets in the simulation, t_n the time coordinate of the nth data set, and t_m the time interval equal to m dynamics time steps. This correlation function provides a convenient means for modeling the time-dependent anisotropic decay of a fluorescent label from an MD simulation. The number of time points averaged, $N - m$, for the correlation function decreases linearly with time. As t_m gets larger, the calculated $r(t_m)$ becomes less accurate; hence the correlation function may be calculated for only half of N data sets.

In a strict sense the use of eq 3 should be limited to the motion of a single fluorescent label attached to a macromolecule (Ichiye & Karplus, 1983; Axelsen *et al.*, 1988, 1991; Chen *et al.*, 1988). Because our MD simulations did not include any such labels, however, we decided to use the pseudo-2-fold axes of the domain dimers to emulate the transition dipole of a typical fluorescent label. There were two compelling reasons for this. First, a domain dimer (either V_L-V_H or C_L-C_H1) can be considered to be a rigid ellipsoid with its long axis collinear to the dimer's pseudo-2-fold axis. Thus, segmental motion of a domain dimer (relative to the whole Fab) will be reflected in the motion of its pseudo-2-fold axis. Second, Fab fragments produced by pepsin cleavage possess a free thiol group at the C-terminus suitable for labeling with a fluorescent probe [see Lim *et al.* (1995)]. A fluorescent label attached to this site will be located at one end of the pseudo-2-fold axis of the constant domain dimer, and a component of its transition dipole will be collinear to the pseudo-2-fold axis.

Decay functions $P_2[\hat{\mu}_a \cdot \hat{\mu}_e]$ for both the variable and constant domain dimers (with and without fluorescein in each case) were calculated with data sets from the last 100 ps of the MD trajectories (Figure 12). Although nearly identical plots were obtained for the variable domain dimer with and without fluorescein, those obtained for the constant domain dimer differed significantly in the presence and absence of fluorescein. This finding was consistent with results obtained from the RDCMs described above and suggested that the constant domain dimer exhibited considerably more segmental motion than the variable domain dimer, at least during the last 100 ps of these simulations.

In order to correlate the above results to our time-resolved fluorescence studies (Lim *et al.*, 1995), extrapolated correlation times (θ) were determined from the decay functions shown in Figure 12 using the following equation, which assumes isotropic decay (*i.e.*, unrestricted rotation of a domain dimer around two laboratory axes that are orthonor-

mal to its pseudo-2-fold axis):

$$P_2 = \exp(-t/\theta) \quad (4)$$

This analysis gave θ values (for $t = 50$ ps) of 8.3 ns for the variable domain dimer both with and without fluorescein, 4.9 ns for the constant domain dimer with fluorescein, and 1.9 ns for the constant domain dimer without fluorescein. Interestingly, the values calculated for the constant domain dimer were 2−3-fold longer than those observed by time-resolved anisotropy measurements (θ values could not be determined experimentally for the variable domain dimer because the fluorescent label was specifically attached to the C-terminus of the constant domain dimer; Lim *et al.*, 1995). We should note that the above calculations are only approximate and that a 5−10-fold longer simulation would be necessary to give accurate predictions. Further, the decay may not be isotropic because the segmental motion of the domain dimers is probably restricted by the switch peptides. For restricted motion, P_2 would decay to a plateau value (S^2, also known as the "order parameter") instead of 0:

$$P_2 = S^2 + (1 - S^2) \exp(-t/\theta) \quad (5)$$

This would have the effect of shortening the above θ values. It was not possible to determine from the water−PBC simulations whether P_2 decayed to 0 or some other plateau value; thus longer simulations are required to determine both the proper decay model and accurate correlation times.

DISCUSSION

The principal conclusion from the MD simulations of the 4−4−20 Fab was that the presence of fluorescein antigen had a significant effect on the dynamics and structure of the Fab. In the absence of fluorescein, motion of the Fab was relatively uncorrelated, and the two domain dimers assumed a bent orientation with respect to each other. In the presence of fluorescein, however, the elbow bend angle between the two domain dimers remained close to that of the X-ray structure, and the motion within each domain was highly correlated, especially the variable domains. Also, although we first thought that the antigen-combining site would collapse in the absence of fluorescein, this was shown not to be the case. In the MD simulation of the Fab without fluorescein, Trp 101L moved into the position previously occupied by fluorescein and essentially restored the volume of the binding site. As mentioned in the introduction, similar motions of tryptophan residues have been observed in the antigen-combining sites of both BV04-01 (Herron *et al.*, 1991) and DB3, a progesterone-binding monoclonal antibody (Arevalo *et al.*, 1993). In these cases, however, the operative tryptophans were located in the H_3 loop, rather than in L_3.

The repositioning of Trp 101L to maintain the volume of the combining site might only be temporary, however, and other nearby residues or solvent molecules may also contribute to the structure of the binding site. For example, water molecules played a key role in restoring the combining site volume. The location of two bound water molecules in the interior of the Fab near the combining site (colored green and light blue in Figure 6) suggests that, in the absence of fluorescein, the site is still open enough to allow movements of water molecules. Additionally, the movement of Trp 101L and other residues in the combining site seemed to affect the structural arrangement of the rest of the Fab, as evidenced by changes in quaternary structure parameters such as elbow bend, plane, and axis angles. Taken together, these observations suggest that the induced-fit mechanism is involved in the binding of fluorescein by the 4−4−20 Fab.

Because the X-ray structure of only the Fab−fluorescein complex was available, fluorescein was removed from the binding site with a "pulling" or dissociating force at the beginning of the second MD simulation. This was highly artificial, as could also be the rapid collapse of the binding site, but perhaps better than simply deleting fluorescein from the ensemble (as was done in the preliminary water shell simulations). The binding (or dissociation) process of a substrate to a host molecule is not yet fully understood and hence difficult to simulate by the method of molecular mechanics; binding is a highly entropic process in which the substrate samples many different configurations near the binding site before the final coupling is made. Novotny and Sharp (1992) showed that the surface of the 4−4−20 Fab surrounding the antigen-combining site possessed a predominantly positive charge. They suggested that the negatively charged fluorescein hapten would form a weak complex with this surface, then move along it, and eventually slip into the hydrophobic binding site. A Monte Carlo simulation of this binding process would make a very interesting project. Previously, a simulation of the dissociation of a diatomic oxygen molecule from myoglobin was performed in which oxygen was pulled away from the heme pocket on a designated reaction path and the binding free energy was estimated (Case & McCammon, 1986). Results suggested that entropic effects dominate the kinetic barrier for the oxygen molecule. Thus, the study of binding processes by simulation can yield important information about molecular interactions, although better methodology still needs to be developed.

Analysis of X-ray structures of different Fab fragments showed that the elbow bend angle is highly variable and that there is no clear evidence that the angle itself is related to antibody function (Sheriff *et al.*, 1988). The present simulations suggest that the dynamics of the elbow bend angle are different for the 4−4−20 Fab with and without the fluorescein ligand and depend upon the degree of lateral interactions between the variable and constant domain dimers. In the liganded Fab, fluorescein became an integral part of the structure and maintained the protein in a specific conformation. For the unliganded Fab, changes in the variable domain structure resulted in a more acute elbow bend angle. The extent of fluctuation of the elbow bend angle, however, could not be completely assessed due to relatively short duration of the simulations, though it seemed that the periodicity of angle fluctuation for the unliganded Fab was longer in time and greater in amplitude. In light of the present MD simulation results, it is possible that the bent conformation of the unliganded 4−4−20 Fab is not favorable for crystal packing. Still, it is unclear what role quaternary structure, and elbow bend angle in particular, plays in the crystallization of Fab fragments. Interestingly, elbow bend angles as low as 140° have been reported in the literature (Davies *et al.*, 1990).

Calculations of cross-correlation maps and decay functions showed that the Fab with fluorescein exhibited a greater degree of concerted motion of residues than the Fab without fluorescein. These maps also showed that the correlations between residues in each of the variable and constant domains were quite high for the Fab with fluorescein but

relatively low between residues of the variable and constant domains. The removal of fluorescein from the binding site caused a significant reduction in coordinated domain motions. Macroscopic observation of this change in the local motion of the Fab is the goal of fluorescence spectroscopy measurements presented in our next paper (Lim *et al.*, 1995); the higher correlated segmental motion of the Fab with fluorescein should result in longer rotational correlation times. Finally, to measure the segmental motion of the Fab on a longer time scale, the size and detail of the molecular system must be reduced substantially. This can be accomplished via Brownian dynamics simulations, from which parameters for direct comparison with fluorescence spectroscopy measurements could readily be calculated (Diaz *et al.*, 1990).

REFERENCES

Alzari, P. M., Spinelli, S., Mariuzza, R. A., Boulot, G., Poljak, R. J., Jarvis, J. M., & Milstein, C. (1990) *EMBO J. 9,* 3807−3814.

Arevalo, J. H., Stura, E. A., Taussig, M. J., & Wilson, I. A. (1993) *J. Mol. Biol. 231,* 103−118.

Axelsen, P. H., Haydock, C., & Prendergast, F. G. (1988) *Biophys. J. 54,* 249−258.

Axelsen, P. H., Gratton, E., & Prendergast, F. G. (1991) *Biochemistry 30,* 1173−1179.

Bedzyk, W. D., Johnson, L. S., Riordan, G. S., & Voss, E. W., Jr. (1989) *J. Biol. Chem. 264,* 1565−1569.

Bedzyk, W. D., Herron, J. N., Edmundson, A. B., & Voss, E. W., Jr. (1990a) *J. Biol. Chem. 265,* 133−138.

Bedzyk, W. D., Weidner, K. M., Denzin, L. K., Johnson, L. S., Hardman, K. D., Pantoliano, M. W., Asel, E. D., & Voss, E. W., Jr. (1990b) *J. Biol. Chem. 265,* 18615−18620.

Berzofsky, J. A. (1985) *Science 229,* 932−940.

Brooks, B. R., Bruccoleri, R. E., Olafson, B. D., States, D. J., Swaminathan, S., & Karplus, M. (1983) *J. Comput. Chem. 4,* 187−217.

Brünger, A. T. (1991) *Annu. Rev. Phys. Chem. 42,* 197−223.

Burt, S. K., MacKay, D., & Hagler, A. T. (1989) in *Computer-Aided Drug Design: Methods and Applications* (Perun, T. J., & Propst, C. L., Eds.) pp 55−91, Marcel Dekker, New York, NY.

Case, D. A., & McCammon, J. A. (1986) *Ann. N.Y. Acad. Sci. 482,* 222−233.

Chen, L. X.-Q., Engh, R. A., Brünger, A. T., Nguyen, D. T., Karplus, M., & Fleming, G. R. (1988) *Biochemistry 27,* 6708−6821.

Dauber-Osguthorpe, P., Roberts, V. A., Osguthorpe, D. J., Wolff, J., Genest, M., & Hagler, A. T. (1988) *Proteins 4,* 31−47.

Davies, D. R., Padlan, E. A., & Sheriff, S. (1990) *Annu. Rev. Biochem. 59,* 439−473.

Diaz, F. G., Iniesta, A., & Garcia De La Torre, J. (1990) *Biopolymers 30,* 547−554.

Dombrink-Kurtzman, M. A., Johnson, L. S., Riordan, G. S., Bedzyk, W. D., & Voss, E. W., Jr. (1989) *J. Biol. Chem. 264,* 4513−4522.

Edmundson, A. B., Ely, K. R., Abola, E. E., Schiffer, M., & Panagiotopoulos, N. (1975) *Biochemistry 14,* 3953−3961.

Gibson, A. L., Herron, J. N., He, X.-M., Patrick, V. A., Mason, M. L., Lin, J.-N., Kranz, D. M., Voss, E. W., Jr., & Edmundson, A. B. (1988) *Proteins 3,* 155−160.

Hanson, D. C., Yguerabide, J., & Schumaker, V. N. (1981) *Biochemistry 20,* 6842−6852.

Hanson, D. C., Yguerabide, J., & Schumaker, V. N. (1985) *Mol. Immunol. 22,* 237−244.

Harte, W. E., Swaminathan, S., & Beveridge, D. L. (1992) *Proteins 13,* 175−194.

Herron, J. N. (1984) in *Fluorescein Hapten: An Immunological Probe* (Voss, E. W., Jr., Ed.) pp 49−76, CRC Press, Boca Raton, FL.

Herron, J. N., & Voss, E. W., Jr. (1983) *Mol. Immunol. 20,* 1323−1332.

Herron, J. N., Kranz, D. M., Jameson, D. M., & Voss, E. W., Jr. (1986) *Biochemistry 25,* 4602−4609.

Herron, J. N., He, X.-M., Mason, M. L., Voss, E. W., Jr., & Edmundson, A. B. (1989) *Proteins 5,* 271−280.

Herron, J. N., He, X.-M., Ballard, D. W., Blier, P. R., Pace, P. E., Bothwell, A. L. M., Voss, E. W., Jr., & Edmundson, A. B. (1991) *Proteins 11,* 159−175.

Herron, J. N., Terry, A. H., Johnston, S., He, X.-M., Guddat, L. W., Voss, E. W., Jr., & Edmundson, A. B. (1994) *Biophys. J. 67,* 2167−2183.

Ichiye, T., & Karplus, M. (1983) *Biochemistry 22,* 2884−2893.

Ichiye, T., & Karplus, M. (1991) *Proteins 11,* 205−217.

Jeffrey, P. D., Strong, R. K., Sieker, L. C., Chang, C. Y. Y., Campbell, R. L., Petsko, G. A., Haber, E., Margolies M. N., & Sheriff, S. (1993) *Proc. Natl. Acad. Sci. U.S.A. 90,* 10310−10314.

Kabat, E. A., Wu, T. T., Perry, H. M., Gottesman, K. S., & Foeller, C. (1991) *Sequences of Proteins of Immunological Interest,* Vol. 1, 5th ed., National Institutes of Health, Bethesda, MD.

Kranz, D. M., & Voss, E. W., Jr. (1981) *Mol. Immunol. 18,* 889−898.

Kranz, D. M., Herron, J. N., Giannis, D. E., & Voss, E. W., Jr. (1981) *J. Biol. Chem. 256,* 4433−4438.

Kranz, D. M., Herron, J. N., & Voss, E. W., Jr. (1982) *J. Biol. Chem. 257,* 6987−6995.

Lim, K., & Herron, J. N. (1991) *Fifth Symposium of the Protein Society,* Baltimore, MD, S48.

Lim, K., Jameson, D. M., Gentry, C. A., & Herron, J. N. (1995) *Biochemistry 34,* 6975−6984.

Novotny, J., & Sharp, K. (1992) *Prog. Biophys. Mol. Biol. 58,* 203−224.

Oi, V. T., Vuong, T. M., Hardy, R., Reidler, J., Dangle, J., Herzenberg, L. A., & Stryer, L. (1983) *Nature 307,* 136−140.

Omelyanenko, V. G., Jiskoot, W., & Herron, J. N. (1993) *Biochemistry 32,* 10423−10429.

Reinitz, D. M., Strich, R., Scott, J. F., & Voss, E. W., Jr. (1988) *Mol. Immunol. 25,* 621−630.

Rini, J. M., Schulze-Gahmen, U., & Wilson, I. A. (1992) *Science 255,* 959−965.

Sheriff, S., Silverton, E., Padlan, E., Cohen, G., Smith-Gill, S., Finzel, B., & Davies, D. R. (1988) in *Structure and Expression* (Sarma, M. H., & Sarma, R. H., Eds.) Vol. 1, pp 49−53, Adenine Press, Schenectady, NY.

Stanfield, R. L., Fieser, T. M., Lerner, R. A., & Wilson, I. A. (1990) *Science 248,* 712−719.

Yguerabide, J., Epstein, H. F., & Stryer, L. (1970) *J. Mol. Biol. 51,* 573−590.

BI942224Y